



Since January 2020 Elsevier has created a COVID-19 resource centre with free information in English and Mandarin on the novel coronavirus COVID-19. The COVID-19 resource centre is hosted on Elsevier Connect, the company's public news and information website.

Elsevier hereby grants permission to make all its COVID-19-related research that is available on the COVID-19 resource centre - including this research content - immediately available in PubMed Central and other publicly funded repositories, such as the WHO COVID database with rights for unrestricted research re-use and analyses in any form or by any means with acknowledgement of the original source. These permissions are granted for free by Elsevier for as long as the COVID-19 resource centre remains active.



Mutations in the coat protein-binding *cis*-acting RNA motifs debilitate RNA recombination of *Brome mosaic virus*

Joanna Sztuba-Solińska^{a,1}, Sean W. Fanning^b, James R. Horn^b, Jozef J. Bujarski^{a,c,*}

^a Plant Molecular Biology Center and the Department of Biological Sciences, Northern Illinois University, DeKalb, IL 60115, USA

^b Department of Chemistry and Biochemistry and The Center for Biochemical and Biophysical Studies, Northern Illinois University, DeKalb, IL 60115, USA

^c Institute of Bioorganic Chemistry, Polish Academy of Sciences, 61-704 Poznan, Poland

ARTICLE INFO

Article history:

Received 6 August 2012

Received in revised form 4 October 2012

Accepted 5 October 2012

Available online 16 October 2012

Keywords:

RNA recombination

Subgenomic RNA

Primer extension

Strand switching

Cis-acting motifs

Coat protein mutants

RNA viruses

ABSTRACT

We have previously described the efficient homologous recombination system between 5' subgenomic RNA3a (sgRNA3a) and genomic RNA3 of *Brome mosaic virus* (BMV) in barley protoplasts (Sztuba-Solińska et al., 2011a). Here, we demonstrated that sequence alterations in the coat protein (CP)-binding *cis*-acting RNA motifs, the Bbox region (in the intergenic RNA3 sequence) and the RNA3 packaging element (PE, in the movement protein ORF), reduced crossover frequencies in protoplasts. Additionally, the modification of Bbox-like element in the 5' UTR region strongly debilitated crossovers. Along the lines of these observations, RNA3 mutants not expressing CP or expressing mutated CPs also reduced recombination. A series of reciprocal transfections demonstrated a functional crosstalk between the Bbox and PE elements. Altogether, our data imply the role of CP in sgRNA3a-directed recombination by either facilitating the interaction of the RNA substrates and/or by creating roadblocks for the viral replicase.

© 2012 Elsevier B.V. All rights reserved.

1. Introduction

Genetic RNA–RNA recombination is the process of joining non-contiguous RNA fragments and is one of the dominant forces shaping the architecture of RNA viral genomes (Sztuba-Solińska et al., 2011b). The process of replicase-driven template switch is the most widely accepted mechanism of recombination (Ranjith-Kumar et al., 2002; Shapka and Nagy, 2004; Hu et al., 2003). Highly structured *cis*-acting replication elements stall the progressing RNA-dependent RNA polymerase (RdRp) complex, which subsequently forces the dissociation of the replicase from the original template and promotes its re-initiation at the acceptor site on another template (Suzuki et al., 2003; Dedepsidis et al., 2010; Draghici and Varrelmann, 2010; Sztuba-Solińska et al., 2011b). Studies with *Brome mosaic virus* (BMV) demonstrated that the homologous crossovers occur near the secondary structures, e.g., within a 3' tRNA-like structure (TLS), which appear to serve as roadblocks for the progression of RdRp. Interestingly, the effects

were more evident during (+)-strand synthesis (Olsthoorn et al., 2002).

Moreover, viral proteins have been shown to affect the distribution of crossover sites (Figlerowicz et al., 1997, 1998; Panaviene and Nagy, 2003) or even to mediate recombination. For example, HIV-1 nucleocapsid protein (NC), an RNA chaperone, not only enhanced homologous strand transfer during reverse transcription but also facilitated the annealing of complementary strands (Negroni and Bus, 2000; Roda et al., 2003). In addition, coronavirus nucleocapsid protein (N) enhanced the frequency of template switching (Zúñiga et al., 2010), and the close association between the protein N and structural protein nsp3 (a component of replicase complex) implied a role in the replicase-driven process (Hurst et al., 2010).

BMV is a tripartite RNA virus, where RNA components 1 and 2 (RNA1 and RNA2) encode, respectively, replicase proteins 1a and 2a, while RNA3 encodes a movement protein (3a) and a coat protein (CP) (Fig. 1). The CP is expressed from subgenomic (sg) RNA4. The multipartite composition of BMV genome and the production of subgenomic RNAs make it a useful model for studies on RNA recombination. Both inter- or intra-segmental crossovers in BMV RNAs were observed at the 3' TLS (Nagy and Bujarski, 1994, 1996, 1997, 1998). Moreover, the RNA3 subgenomic promoter (sgp) was mapped as an active recombination hot-spot (Wierzechowski et al., 2004), additionally engaged in the formation of nonreplicating 5' subgenomic RNA3a (sgRNA3a) (Wierzechowski et al., 2006).

* Corresponding author at: Plant Molecular Biology Center and the Department of Biological Sciences, Montgomery Hall, Northern Illinois University, DeKalb, IL 60115, USA. Tel.: +1 815 7530601; fax: +1 815 753 7855.

E-mail address: jbujarski@niu.edu (J.J. Bujarski).

¹ Current address: HIV Drug Resistance Program, National Cancer Institute NCI-Frederick, P.O. Box B, Frederick, MD 21702-1201, USA.

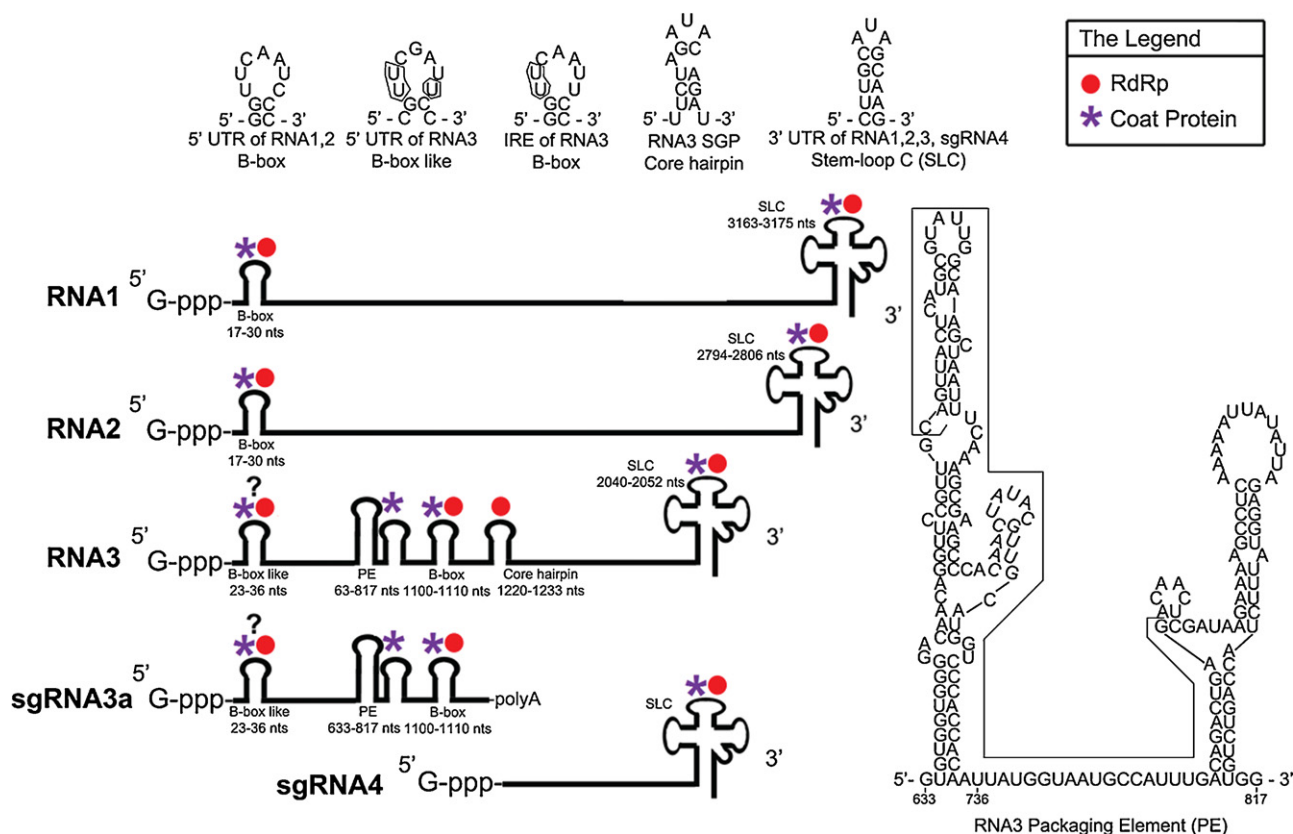


Fig. 1. Binding of BMV CP molecules to the RNA3 elements. This schematic summarizes the secondary elements on BMV RNAs known to serve as binding sites to either CP or RNA-dependent RNA-polymerase (RdRp) proteins. BMV genomic RNAs are represented as thick black lines with the 5' cap structure and 3' tRNA-like element shown at the ends. CP is indicated with a purple asterisk, while RdRp is represented as a red circle. The names for each binding site are shown below with exact nucleotide positions. The predicted secondary structures (with MFOLD) are represented on the top of the diagram. Sequences altered in the RNA mutants tested are indicated by solid boxes. The question marks above the 5' UTR Bbox-like elements indicate the potential, unconfirmed CP/RdRp binding(s).

Recently, we reported the efficient homologous recombination between BMV sgRNA3a and genomic RNA3 in barley protoplasts (Sztuba-Solińska et al., 2011a). Both *in vitro* and *in vivo* data suggested that the exposed 3' terminal polyA tail of sgRNA3a can prime the extension of (+) strand RNA synthesis on the (–) sense RNA3 templates. In addition, more upstream regions also supported homologous crossover events, most likely by internal strand transfers during (–) sense RNA synthesis.

Among the *cis*-acting motifs known to bind BMV CP (Fig. 1), the Bbox element is located within the intercistronic region of the RNA3 (+) strand as part of the intergenic replication enhancer (IRE) (Pogue et al., 1992; Baumstrak and Ahlquist, 2001). Another motif is a highly structured position-dependent RNA3 packaging element PE that is localized between nucleotides (nts) 550 and 820 and is considered as a selective domain for CP interaction facilitating specific packaging of BMV RNA3 (Choi and Rao, 2003). Since sgRNA3a represents an exact copy of the 5' half of (+) strand RNA3, it also carries these two *cis*-acting elements. In this work, we show that sequence alterations within both motifs, either on RNA3 and/or on the sgRNA3a components, diminished the recombination frequency in protoplasts. A series of reciprocal transfections revealed putative interactions between these motifs in establishing the crossover locations. Moreover, the transfection of protoplasts with the RNA mutants incapable of CP expression or that expressed the CP variants with altered domains recognizing the CP-binding motifs also reduced the recombination frequency. Our study offers *novel insight* into BMV RNA recombination and indicates that associations of CP with the RNA *cis*-acting motifs can mediate RNA recombination process.

2. Materials and methods

2.1. Materials

Full-length cDNA clones, corresponding to wt BMV RNAs 1, 2, and 3 (Russian strain) were obtained from P. Ahlquist laboratory as plasmids pB1TP3, pB2TP5, and pB3TP7, respectively (Janda et al., 1987). The plasmids were used as templates to synthesize the capped full-length transcripts *in vitro* using the MEGAScript T7 kit (Ambion, Austin, TX). Moloney murine leukemia virus (MMLV) reverse transcriptase, *Pfu* DNA polymerase (Agilent Technologies), restriction enzymes, and dNTPs were obtained from the Promega Corporation or New England Biolabs, Inc.

2.2. Generation of RNA3 and sgRNA3a variants

All RNA3 variants were PCR-amplified from plasmid pB3TP7 using the primers listed in [supplementary Table 1](#). Primer 1 was used to introduce the 5' A to U substitution at nt position 2, which was shown to increase both the (–) strand RNA3 production (Hema and Kao, 2004) and the frequency of RNA3–sgRNA3a crossovers (Sztuba-Solińska et al., 2011a).

The Bbox-RNA3 derivative carrying UU to AA substitutions at nts 1102–1103 was generated using fusion PCR. The 5' segment was generated with primers 1 and 2, whereas the 3' segment was generated with primers 3 and 4 followed by PCR amplification using both fragments and primers 1 and 4. Similarly, the Δ PE-RNA3 variant was generated using fusion PCR with flanking primers 1 and 4 of the 5' fragment (synthesized using primers 1 and 5), carrying

the PE deletion (nt 660–762) and the 3' fragment (synthesized with primers 6 and 4).

The 5'box-RNA3 construct carried U to A substitutions at nt 23–24 and nt 29, which were generated using single-step PCR with primers 7 and 4. The CP0-RNA3 construct carried a G to C substitution at position 1242 and an A to C substitution at position 1239, which were both generated using primers 8 and 9. Subsequently, the PCR products were purified using the Qiaquick® PCR Purification Kit (Qiagen), digested with *Pfl*MI (nt 816) and *Sall* (nt 1254) enzymes and re-ligated between the *Pfl*MI and *Sall* sites into pB3TP7. The resulting product was used as template for the next round of PCR with primers 1 and 4.

The CP-Bbox RNA3 construct expressing the CP derivative carrying alanine substitutions within the aa residues T145, D148, N151, Y155, Y157, S159, V162, P163, and K165, was created using fusion PCR with primers 1 and 10 for the 5' fragment (carrying the desired mutations plus the 5' A to U substitution at nt position 2) and primers 11 and 4 for the 3' fragment. Subsequently, the overlapping segments were mixed and co-amplified in the next round of PCR using primers 1 and 4. Likewise, the CP-SLC construct carrying alanine substitutions within the CP aa residues V27, P29, V30, V32, P34, Q39, and K41 was created using fusion PCR with flanking primers 1 and 4 and two fragments: the 5' fragment (generated with primer 1 and 12; the latter carrying the desired mutations plus the 5' A to U substitution at nt position 2) and the 3' segment (obtained with primers 13 and 4).

The previously published pJS-22 plasmid (Sztuba-Solińska et al., 2011a) was used as a template to generate sgRNA3a derivatives: SG, Bbox-SG, ΔPE-SG, 5'box-SG using fusion PCR with primers specific for each corresponding RNA3 derivative (indicated above). For each construct, the obtained PCR product was digested with *Bgl*II to transcribe the full-length sgRNA3a. These sgRNA3a-derived transcripts carried the polyA tail plus four extra bases (GAUC) at the 3' end.

The cDNA templates comprising either the Bbox (Fr Bbox) or the PE (Fr PE) fragment RNA3 sequences were synthesized using PCR amplification of the above corresponding full-length RNA3 cDNA clones (wt or mutated) with the following oligonucleotides (supplementary Table 1): primers 27 and 28 for the Bbox Fr (nts 1070–1140) and primers 29 and 30 for the PE Fr (nts 633–817). The cDNA templates were subsequently transcribed *in vitro* in the presence of alphaP³²-CTP, and the unincorporated radioactivity was removed on a Sephadex G-25 spin minicolumn. Radioactive RNA3 probes were used for the RNA-CP filter binding assays (below).

The cDNA templates for the synthesis of wt and mutated variants in the *cis*-acting RNA motifs were generated from the corresponding RNA3 cDNA derivatives using one-step PCR with primers 21 and 22 for the intergenic Bbox motif, 23 and 24 for the packaging element (PE), and 25 and 26 for the 5' Bbox related region.

The final cDNA templates were sequenced to confirm their correct assembly. Subsequently, the RNAs were synthesized *in vitro* using the MEGAscript T7 kit (Ambion, Austin, TX) and purified using MicroSpin™ G-50 columns (GE Healthcare).

2.3. Protoplast assays

Barley mesophyll protoplasts were isolated from the five-day-old barley seedlings according to the protocol of Rao (2007) with modification performed in our laboratory (Sztuba-Solińska et al., 2011a). On average, one million protoplast cells were inoculated with 1 μg of each desired combination of the *in vitro*-capped transcripts using a PEG-mediated transfection protocol, as described previously (Sztuba-Solińska et al., 2011a).

2.4. RT-PCR and cloning

Total RNA extracted from protoplast samples was separated in denaturing 1.2% agarose gels (Sambrook and Russell, 2001). The RNA3-size material was cut out from the gel and purified using spin columns (Ambion, Cat# 605 AM10065) followed by chloroform extraction and ethanol precipitation. The final RNA preparation was subjected to RT-PCR with primers 17 and 18 (supplementary Table 1) and the products were purified with the Qiaquick® PCR Purification Kit (Qiagen) and cloned into the pGEM-T Easy VectorSystem (Promega). The resulting clones were analyzed by restriction digestion.

2.5. Northern blot analyses

The accumulation of BMV RNAs in protoplasts was detected using northern blotting (Kroner et al., 1989). The blots of the total RNA extracts (see above protocol) were hybridized with a probe specific to the 200 nts at the 3' end of the (+)-strand RNA as described previously (Wierchoslawski et al., 2004). The hybridization signals were quantified on scanned X-ray films using ImageQuant 5.0 software from Amersham Biosciences.

2.6. RT-PCR controls

To verify that the recombinant RNAs emerged during RNA replication rather than during RT-PCR (Cocquet et al., 2006), protoplasts were co-transfected with a mixture of wt BMV RNA3 and SG construct, but without wt RNAs 1 and 2. Another control involved the RT-PCR amplification of the RNA3 sequences from a mixture of wt BMV RNAs and SG construct, omitting the protoplast transfection. The RNA transcripts used in these experiments were pre-treated with an excess of RNase-free DNase (Ambion) to remove the plasmid DNA template and prevent the occurrence of DNA-amplified PCR products. Subsequent analyses of cDNA clones did not detect RNA3 recombinants (not shown). In yet another control, total RNA was extracted from protoplasts that were transfected with wt (virion) BMV RNA. No false positive recombinants were identified.

2.7. Expression and purification of BMV CP variants

The wild type and mutated CP sequences were amplified from pB3TP7 plasmid or from the corresponding fusion PCR products: CP-Bbox and CP-SLC (described above) using primers 19 and 20 that carried, respectively, the *Bam*HI and *Xho*I restriction sites. The PCR products were digested with restriction enzymes and re-ligated into the corresponding sites on the pET21a(+) expression vector (EMD Biosciences). The resulting constructs were transformed in *Escherichia coli* BL21 (DE3) cells. Following a 5 ml overnight incubation at 37 °C, a 50 ml LB/amp subculture was inoculated with 1 ml of the overnight culture. Once at mid-log phase growth (O.D.₆₀₀ = 0.6), the subculture was used to inoculate a 1 L LB/amp culture. The expression of the BMV-CPs was induced with 0.1 mM IPTG once the cells reached mid-log phase. After 3 h incubation at 37 °C, the cells were harvested by centrifugation at 8000 × g for 15 min. The pellet was resuspended in 10 mM Tris/pH 8 and sonicated for 4 one min on/off cycles with a Model 60 Sonic Dismembrator (Fisher Scientific) at an output power of 21 W. The lysed cells were centrifuged at 22,700 × g for 15 min, and the supernatant fraction was loaded onto a Histrap HP column (GE Healthcare), and the column was washed with 20 mM imidazole, 50 mM phosphate and 500 mM NaCl pH 7.4. The protein was eluted with 500 mM imidazole, 50 mM phosphate and 500 mM NaCl pH 7.4, and further purified on a HiLoad 26/60 Superdex 75 prep grade FPLC column

(10 mM Tris, 150 mM NaCl, pH 8.0). Finally, the protein was dialyzed in a buffer containing 50 mM Tris–HCl, pH 7.5, 300 mM NaCl and 1 mM DTT to keep the molecules in a monomeric stage (Yi et al., 2009b).

2.8. Filter-binding assays for CP–RNA interactions

Purified wt or mutant CP preparations (200 ng) were incubated with serial dilutions of 1 nM of radiolabeled RNAs (ratios 1:0; 1:10; 1:100 and 1:1000) in the RNA binding buffer (50 mM Tris–HCl, pH 7.5, 50 mM NaCl and 4 mM MgCl₂, as described in Yi et al., 2009a), in a total volume of 20 μl. Two microliters of each reaction mixture were applied on the nitrocellulose membrane, irradiated with UV at 1000 mJ for 2 min, dried, washed with the binding buffer, dried again and the retained radioactivity was visualized using autoradiography on an X-ray film.

3. Results

3.1. The PE element and sgRNA3a–RNA3 recombination

The previously described barley protoplast recombination system (Sztuba-Solińska et al., 2011a) involved wt BMV RNAs 1 and 2, and wt or modified RNA3 and sgRNA3a. Recombination events were tracked based on the inheritance of three restriction marker mutations (*Bam*HI, *Hind*III and *Pst*I) located within the 3a ORF and near the 5' and 3' sides in all the sgRNA3a constructs (Fig. 2). The marker mutations were translationally silent, stable, and they did not affect the accumulation of progeny RNA3 recombinants in protoplasts (Sztuba-Solińska et al., 2011a). Moreover, all of the RNA3 constructs that were used contained a 5' A to U substitution at nt 2, which was shown previously to decrease the accumulation of (+) RNA3 strands without affecting (–) strands (Hema and Kao, 2004). In our previous study, this particular substitution was

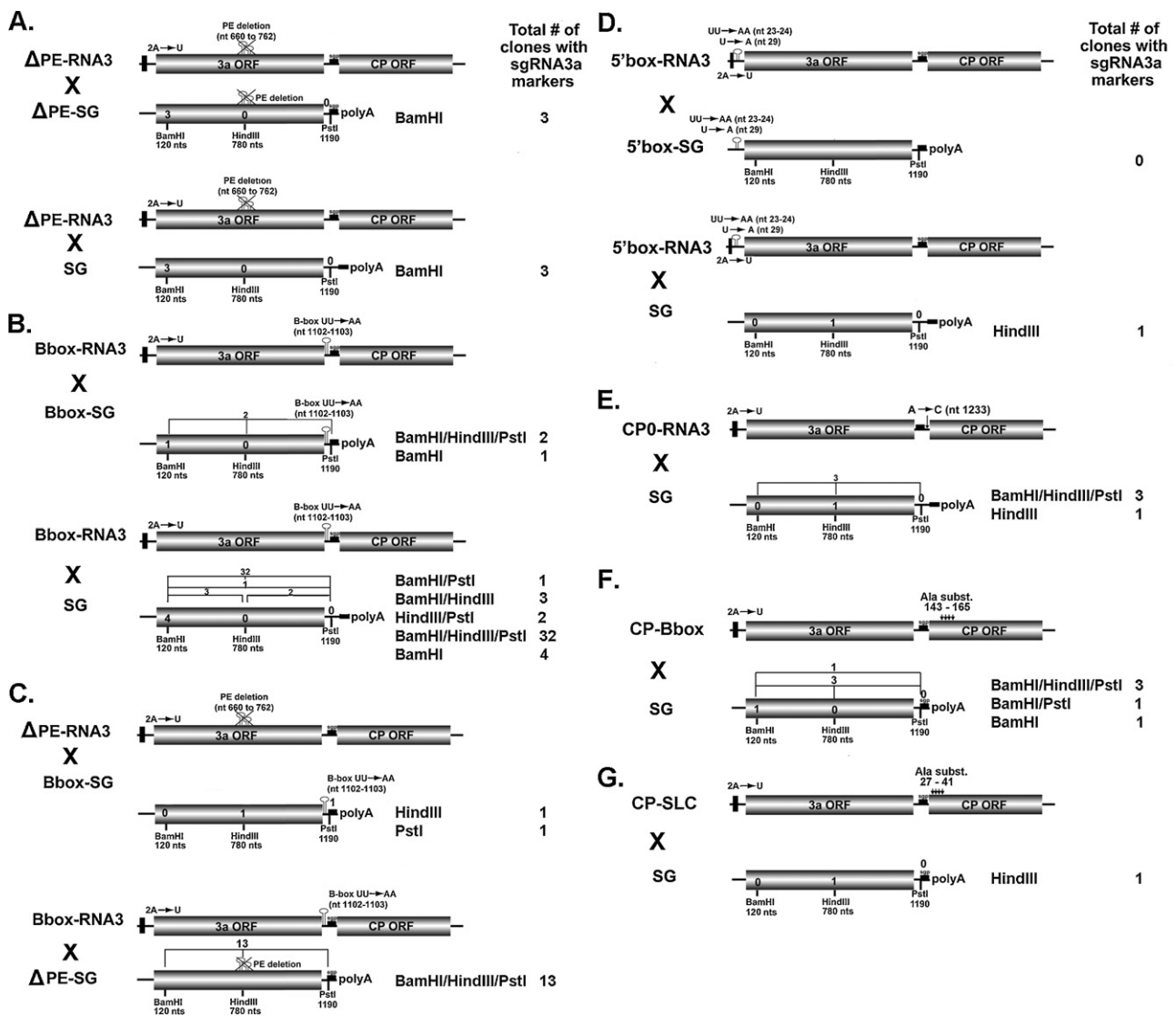


Fig. 2. The distribution of crossover sites between recombining RNA3 and sgRNA3a derivatives in co-transfected barley protoplasts. The RNA3/sgRNA3a inocula are indicated on the left of each transfection experiment panel (for further description of the RNA constructs, see Section 2). All RNA3 derivatives bear a point mutation (A to U) at nt position 2 near the 5' end (black square) to lower the production of (+) sense RNA3. The positions of marker restriction sites are indicated below each construct. The column on the right shows the number of recombinants bearing the indicated restriction marker sites identified among 100 insert-bearing cDNA clones; the rest of cDNA clones represented the wt input RNA3 sequence. These numbers are repeated inside the shaded rectangles (for recombinants with single markers) or above the brackets (for recombinants with multiple markers). The numbers summarize the results from two independent transfection experiments per each combination of the inoculated RNA substrates. To calculate total recombination frequency, the number of all recombinant-bearing clones should be summarized and divided by 100.

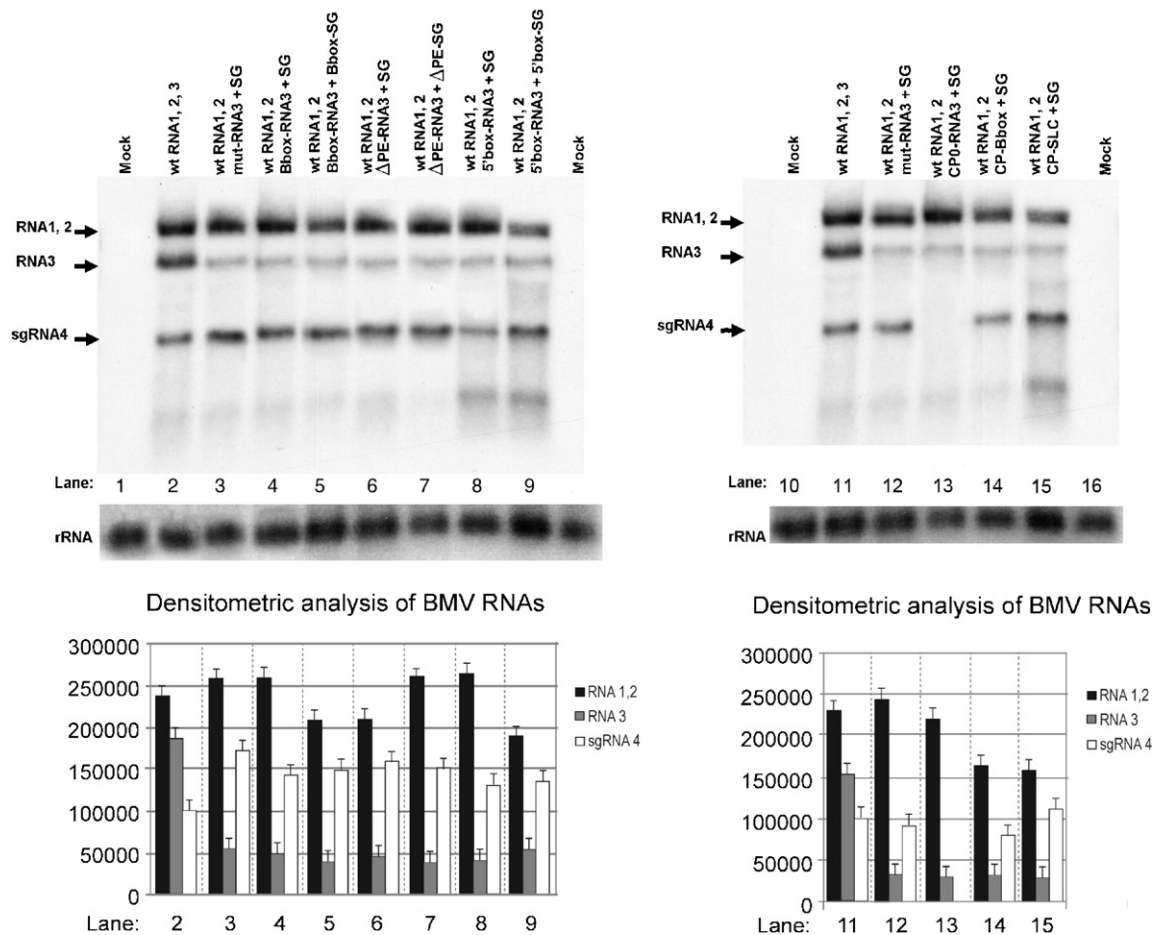


Fig. 3. The accumulation of BMV RNAs in transfected barley protoplasts. The protoplasts were transfected with RNA3 and sgRNA3a derivatives plus the wt RNAs 1 and 2. Total protoplast RNA was extracted after 48 h post inoculation, separated on a 1.2% denaturing agarose gel, blotted and probed with the 3' RNA probe (see Section 2). Lanes 1 and 10, mock-inoculated protoplasts as the negative control; lanes 2 and 11, protoplasts transfected with wt BMV RNAs 1, 2 and 3 as positive controls; lanes 3–9, and 11–15, protoplasts co-transfected with different combinations of RNA3 and sgRNA3a variants (shown on top). Below, digital bands were analyzed with ImageQuant (*GE-Healthcare*), and the measured areas were defined as absolute intensity. These numbers were used to calculate the relative intensity of each band. The mean from multiple experiments was used to plot the graph. Error bars represent the calculated standard errors.

also shown to increase RNA3–sgRNA3a crossovers in protoplasts, as well as it kept the (+) RNA3 strand synthesis at lower level (mut-RNA3) (Sztuba-Solińska et al., 2011a). Since mut-RNA3 recombined with sgRNA3a (SG) at elevated frequency (42%), we hypothesized that sgRNA3a primed RNA recombination on (–) sense RNA3 templates.

The Δ PE-RNA3 construct, in addition to the A to U mutation, it also carried PE deletion (nts 660–762), whereas the Δ PE-SG sgRNA3a construct, besides containing the same deletion, it contained three previously described silent restriction marker mutations (*Bam*HI, *Hind*III and *Pst*I, see Fig. 2). These marker mutations allowed mapping of the recombination sites within the 5' region of RNA3 and were present in all the sgRNA3a-derived constructs used in this work (Sztuba-Solińska et al., 2011a). The Δ PE-RNA3 and Δ PE-SG constructs were co-transfected (together with wt RNA1 and 2) into barley protoplasts (Fig. 2A). Only three recombinant clones were identified among 100 RT-PCR-generated cDNA clones, thus the recombination frequency (3%) was greatly reduced as compared to the previously published results for mut-RNA3 and SG co-transfection (42%) (Sztuba-Solińska et al., 2011a). The control amplifications did not show RT-PCR generated recombinants (see Section 2). The three characterized clones all carried the 5'-most *Bam*HI marker mutation which implied that the residual RNA3–sgRNA3a crossovers occurred within the regions 5' upstream to PE element.

In yet another experiment, the Δ PE-RNA3 derivative was co-transfected with SG construct (Fig. 2A). Similarly, the recombination frequency approached only 3%, with three recombinant RNA3 clones containing the 5' *Bam*HI marker site, implying internal strand switching. Again, the level of RNA3 (Fig. 3, lane 6) was alike that of mut-RNA3, reflecting an equal availability of RNA3 substrate for crossovers. Overall, when compared with the 42% frequency between mut-RNA3 and SG, the lack of functional PE in RNA3 effectively reduced the recombination frequency to a marginal value, demonstrating the importance of the PE motif. However, the presence of the PE region in the sgRNA3a donor did not seem to be critical because both SG and PE-SG recombined at comparably low rate.

3.2. The Bbox motif and sgRNA3a-RNA3 recombination

A structured region near the 3' sgRNA3a polyA tail, referred to as the intergenic Bbox motif, participates in the assembly of the BMV replicase complex on RNA3 via interactions with protein 1a (Baumstrak and Ahlquist, 2001), and it binds CP molecules via a specific peptide domains, as mapped by Yi et al. (2009b). To determine whether Bbox structure contributes to RNA3–sgRNA3a crossovers, UU to AA substitutions previously found to lower the affinity for BMV CP (Yi et al., 2009a) were introduced within the Bbox hairpin loop (Fig. 1). Co-transfection with a mixture of Bbox-RNA3

and Bbox-SG generated only three RNA3 recombinants (per 100 cDNA clones analyzed): two clones contained all three marker sites, whereas one clone contained only the 5' *Bam*HI site.

In a separate experiment, the Bbox-RNA3 was co-transfected with SG construct to determine whether the presence of the wt Bbox motif in sgRNA3a could rescue the previously reported high recombination frequency for unmutated RNAs. Indeed, among 100 cDNA clones, there were 42 recombinants (Fig. 2B), of which the majority carried all three marker restriction sites (74%, 32 clones), while few had either single (*Bam*HI – four clones) or double (*Bam*HI/*Hind*III – three clones, *Bam*HI/*Pst*I – one clone, *Hind*III/*Pst*I – two clones) restriction sites. This distribution of crossovers suggested that the recombination was mainly governed via the incorporation of sgRNA3a (referred to as primer extension). Here, the unchanged 3' end motifs of sgRNA3a, the 3' polyA tail and Bbox, would efficiently prime the (+) sense RNA3 synthesis.

3.3. Reciprocal Δ PE-Bbox co-transfections

Next, we examined the potential interplay between the PE and Bbox motifs. The co-transfection of protoplasts with the Δ PE-RNA3 and Bbox-SG constructs resulted in only two recombinants: one containing the central *Hind*III site and one with the 3' *Pst*I site (Fig. 2C). Thus, the absence of PE in RNA3 along with the Bbox mutation in sgRNA3a minimized the crossover frequency. However, the reverse arrangement (Bbox-RNA3 and Δ PE-SG) supported a 13% recombination frequency (Fig. 2C). In this case, all recombinants contained three marker mutations. These results suggested that the disrupted interaction of CP with the RNA3 Bbox lowers the frequency of internal crossovers, while the presence of unchanged 3' end motifs, in particular the Bbox in sgRNA3a supports the incorporation of full-length sgRNA3a during synthesis of progeny (+) sense RNA3 molecules.

3.4. The 5' Bbox-like motif and sgRNA3a-RNA3 recombination

Previous studies implied that the 5' UTR region was another possible RNA3–sgRNA3a recombination hotspot (Sztuba-Solińska et al., 2011a). The 5' Bbox-like motif was mutated by replacing U with A residues at nt positions 23–24 and at nt position 29 in order to change its 7-nt hairpin-loop sequence (Fig. 1, top). The resulting 5' box-RNA3 and 5' box-SG constructs (Fig. 2D) did not generate any recombinants in protoplasts. Likewise, the 5' box-RNA3 \times SG (Fig. 2D) produced only one recombinant per 100 clones analyzed, and it carried the internal *Hind*III site. Thus, the intact 5' UTR of RNA3 seems to be required for efficient crossovers. We conclude that the 5' UTR must participate in the recombination activity of the RNA3 template.

3.5. Effect of mutations within the BMV CP ORF on recombination

The BMV CP was shown previously to specifically bind not only to Bbox and PE elements (Rao, 2006; Yi et al., 2009a,b) but also to stem-loop C (SLC) of the 3' TLS in RNA3 (Fig. 1). The CP domains responsible for the binding to Bbox and SLC motifs were mapped (Yi et al., 2009b). To address whether the absence of CP affects sgRNA3a–RNA3 recombination, CP0-RNA3 was created. CP0-RNA3 did not transcribe sgRNA4 due to mutations introduced within the sgRNA4 promoter region (+1 G to C and –2 A to C), as previously reported (Sivakumaran et al., 2004), and thus in the above system the expression of CP is debilitated. The results of disrupted sgRNA4 transcription along with an unaffected level of RNA3 accumulation in protoplasts are shown in Fig. 3 (compare lanes 12 and 13). Among four identified recombinants (per 100 analyzed cDNA clones), three acquired a complete set of SG-derived restriction markers, while one clone inherited only the central *Hind*III and the 3' *Pst*I sites

(Fig. 2E). This suggested that the remnant recombination activity could occur via extension of sgRNA3a serving as a primer during copying of progeny RNA3.

To test this idea further, two previously mapped specific RNA binding domains on CP (Yi et al., 2009b) were mutated, including critical amino acid regions 143–165 (Bbox motif binding domain) and 27–41 (the 3' SLC stem-loop binding domain). Since the PE binding domain was not mapped on BMV CP molecule, the corresponding amino acids could not be mutated. Two CP derivatives were generated: the CP-Bbox mutant carrying alanine substitutions for residues T145, D148, N151, Y155, Y157, S159, V162, P163 and K165, and the CP-SLC variant carrying alanine substitutions for residues V27, P29, V30, V32, P34, Q39 and K41. To examine recombination frequency, both RNA3 CP mutants were co-transfected separately with SG in barley protoplasts. The CP-Bbox RNA3 generated the following recombinants: three carrying all sgRNA3a marker restriction sites (likely reflecting sgRNA3a extension on progeny RNA3), one carrying the 5' *Bam*HI and the 3' *Pst*I sites, and one carrying only the 5' *Bam*HI site (Fig. 2F). In the case of CP-SLC RNA3, only one recombinant emerged, containing the inner *Hind*III site (Fig. 2G). Taken together, these results revealed that either the elimination of CP expression or the disturbed CP binding to *cis*-acting motifs on the RNA substrates, or both, inhibited the RNA3–sgRNA3a recombination.

3.6. Accumulation of mutant BMV RNAs in protoplasts

To determine if sequence modifications affected the accumulation of BMV RNA3 and/or sgRNA3a substrates in host cells, barley protoplasts were co-transfected with transcripts of RNA3 and sgRNA3a (1:1 molar ratio) along with wt RNAs 1 and 2. The subsequent Northern blot analysis of total RNA extracts confirmed previously reported observations (Hema and Kao, 2004; Sztuba-Solińska et al., 2011a); a noticeable reduction in the production of (+) strands was observed in all mutated RNA3 variants that carried the A to U substitution in their 5' noncoding regions (lanes 3–9 and 12–15 in Fig. 3), with all RNA3 and sgRNA3a derivatives accumulating to levels comparable with the control inoculum (Fig. 3, lanes 3 and 12). Moreover, the addition of full-length sgRNA3a (SG construct) (Fig. 3, lanes 4, 6, 8, 12, 13, 14, and 15) did not affect the ratio of accumulating BMV RNA components versus the control inoculum (Fig. 3, lane 3 and 12), and the ratios of BMV RNAs were not affected by mutations introduced within the CP ORF (Fig. 3, lanes 13, 14, 15) as compared to the control transfection with BMV RNA1 and 2, mut-RNA3 and full-length sgRNA3a (SG construct) (Fig. 3, lane 3 and 12). Furthermore, the CP0-RNA3 mutant did not produce sgRNA4 as expected (Fig. 3, lane 13), and the addition of the SG construct did not markedly influence the accumulation of the remaining BMV RNA components. Overall, we concluded that the observed differences in the recombination frequencies and in the distribution of crossover sites were not due to the altered stability or distorted accumulation of the tested RNA derivatives.

3.7. The stability of RNA3 and sgRNA3a derivatives in protoplasts

To determine whether the altered stability of transfected RNA substrates affected the observed crossover frequencies in protoplasts, stability assays were performed as previously described (Sztuba-Solińska et al., 2011a). Various combinations of the transcribed genomic RNA3 and sgRNA3a radioactive variants were co-transfected into barley protoplasts along with unlabeled RNA1 and 2. The protoplasts were thoroughly washed to remove the untransfected radioactive material, and the total RNA was extracted at three time points. The stabilities of the RNA3 and sgRNA3a variants were assessed in comparison with the previously tested wt RNA3 and wt sgRNA3a transcripts. All of the transcript variants were

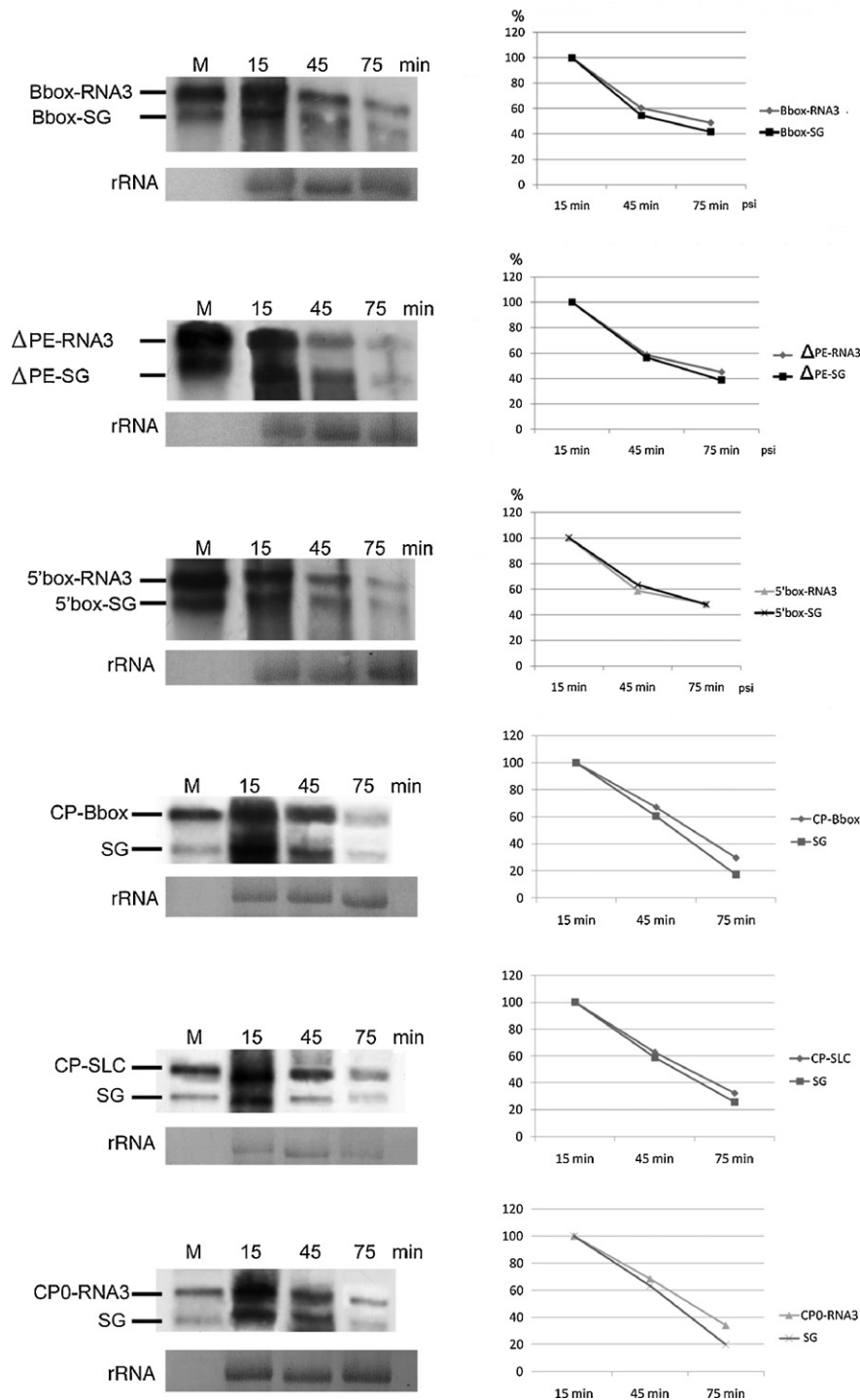


Fig. 4. The stability of the RNA3 and sgRNA3a constructs used in protoplast co-transfection experiments. Left. Autoradiogram representing the intensity of bands corresponding to mixtures of radioactive RNA3 and sgRNA3a variants that were co-transfected (together with nonradioactive RNAs 1 and 2) into protoplasts and extracted after incubation for 15, 45, or 75 min. M marks the lane where the input RNA3 and sgRNA3a radioactive transcript constructs were run as size standards; the positions and names of the constructs are indicated on the left-hand side. Right. The results of densitometric analysis of the bands shown in A, calculated as the percentage of the initial band intensity. The experiments were repeated twice to average the obtained results (Sztuba-Solińska et al., 2011a).

stable to a similar degree within the 75 min assay time (Fig. 4), indicating that the observed frequencies during the protoplast assays reflected recombination rates rather than altered RNA stability.

3.8. RNA-CP binding in vitro

To determine whether the lack of recombination activity correlated with diminished CP-RNA3 binding, both the wt and two BMV

CP mutants were expressed in *E. coli* and purified as described in Methods section. A single band corresponding to CP was identified after sodium dodecyl sulfate polyacrylamide gel electrophoresis (SDS-PAGE) (shown in Fig. 1 Supplement).

The affinity of these CP mutants to the RNA3 templates was analyzed with filter-binding assays. Equimolar concentrations of serially diluted (1; 1:10; 1:100; 1:1000) radioactive wt or mutated RNA3 probes (comprising the regions of individual *cis*-acting

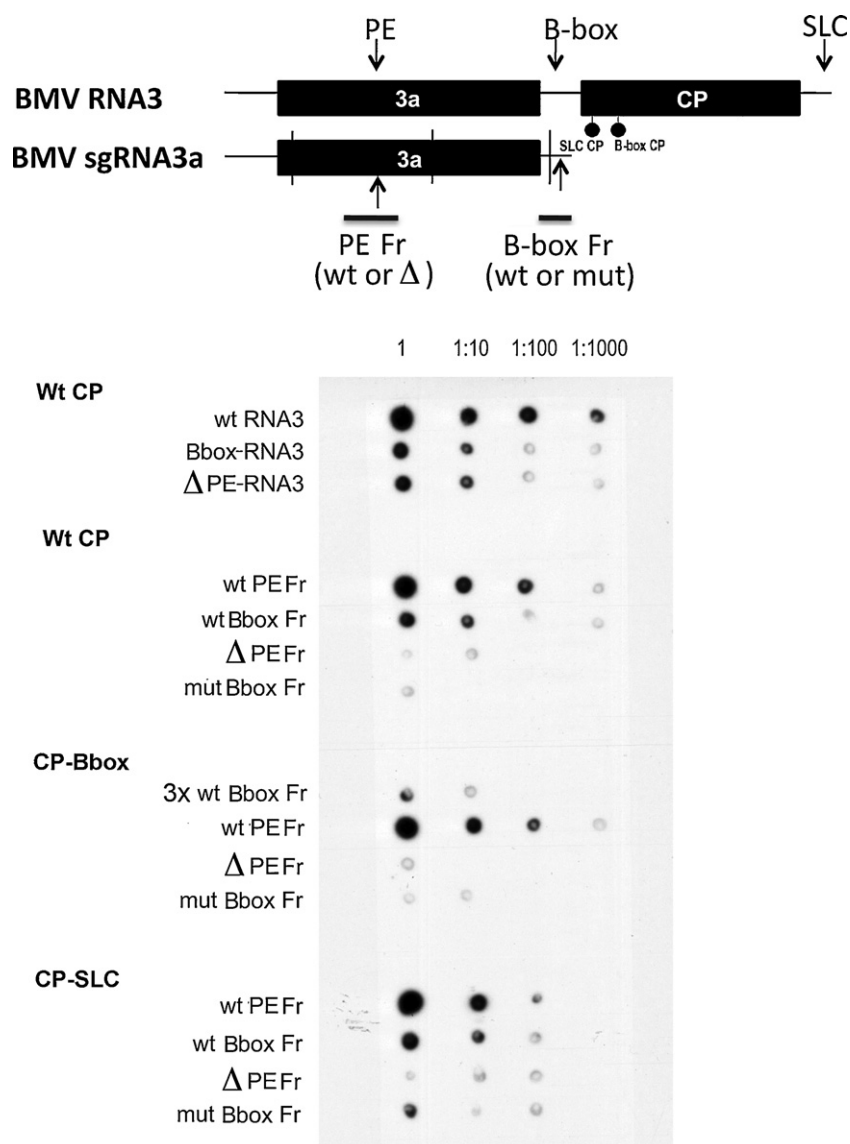


Fig. 5. Filter binding assays for BMV CP–RNA interactions. The CP–RNA complexes were loaded onto nitrocellulose membrane and subjected to autoradiography, as described in Section 2. The individual CP/RNA combinations are indicated on the left-hand side, whereas the dilutions of the radioactive RNA probes are marked on the top. The location of marker restriction sites on sgRNA3a component is depicted as short vertical thin lines. The positions of PE, Bbox and SLC cis-acting elements known to bind BMV CP are marked by arrows above RNA3 molecule. The RNA3 fragments used as radioactive binding probes are represented by short black lines under sgRNA3a molecule and marked as PE Fr or B-box Fr, respectively. In addition, the regions of the amino acid substitutions in the SLC CP and Bbox CP mutants are shown as black dots right below the CP ORF of RNA3.

sequences, as shown on top of Fig. 5), were incubated with equimolar wt or mutated CP preparations. The complexes were transferred onto nitrocellulose filters, washed, and the bound radioactivity was determined *via* autoradiography. As shown in Fig. 5, the wt CP bound efficiently to wt and mutated full-length RNA3 probes (top section), as well as to wt PE (wt PE Fr) and to wt Bbox (wt Bbox Fr) RNA3 fragments (Fig. 5, second section, lines 1 and 2), because the interaction was at the detectable level even with 1:1000 diluted probe. This reflected the fact that more than one CP peptides were found to be cross-linked to the BMV RNAs by using the reversible cross-linking and peptide fingerprinting (RCAP) assays (Yi et al., 2009b). However, the deleted Δ PE (Δ PE Fr) and mutated Bbox (mut Bbox Fr) RNA3 fragments interacted at least 100 fold less efficiently with wt CP (Fig. 5, second section, lines 3 and 4, respectively) as the 1:10 diluted probes barely generated detectable signal. Likewise, the CP variant with mutated peptide recognizing Bbox motif (CP-Bbox) also bound inefficiently to both Δ PE Fr and mut Bbox Fr probes (Fig. 5, third section, lines 3 and 4, respectively) and to

an increased (three-fold) amount of wt Bbox Fr probe (line 1), yet binding to wt PE Fr was reasonably high (Fig. 5, line 2). This analysis revealed separate PE and Bbox binding sites on the CP molecule, which is consistent with the previously published data of Yi et al. (2009b). The CP-SLC mutant bound with relative efficiency to both wt PE and Bbox Fr (Fig. 5, bottom section, lines 1 and 2) but it bound with much less efficiency to the PE and Bbox mutated counterparts (Fig. 5, lines 3 and 4). Collectively, our data suggest that all three RNA3 motifs interact with separate regions on the BMV CP molecule, and confirm that the inhibition of CP binding parallels the diminished RNA3–sgRNA3a recombination frequency.

4. Discussion

Both RNA secondary structures and protein factors participate during RNA recombination in BMV (Bujarski and Dzianott, 1991; Nagy and Bujarski, 1993; Figlerowicz, 2000; Olsthoorn et al., 2002; Panaviene and Nagy, 2003) and in other RNA viruses (Suzuki et

al., 2003; Dedepsidis et al., 2010; Draghici and Varrelmann, 2010; Zúñiga et al., 2010). Here, we report about coat protein-binding *cis*-acting RNA motifs as essential factors supporting RNA3–sgRNA3a homologous recombination in BMV system.

The starting point of our analysis was the recombination frequency between mut-RNA3 and SG construct (wt sgRNA3a sequence carrying three additional silent marker mutations) that previously reported to be at high 42% level (Sztuba-Solińska et al., 2011a). The mut-RNA3 × SG experiment generated only six recombinants with more random distribution of three markers; thirteen carrying *Bam*HI–*Pst*I double markers; one and two carrying (respectively) *Bam*HI–*Hind*III or *Hind*III–*Pst*I double markers; and eleven, one, and eight carrying (respectively) *Pst*I, *Hind*III, or *Bam*HI single markers. This suggested that crossovers happened near the 3' end of sgRNA3a or more internally, likely near the PE encapsidation region. Based on prior and current studies we speculated that recombination occurred by two mechanisms (Fig. 6A and B): (1) sgRNA3a-directed primer extension on (–) strand RNA3, where the exposed 3' terminal regions of sgRNA3a would promote the template switch during (+) strand RNA synthesis, or by (2) strand switching between (+) strands [during (–) strand synthesis] which could engage internal secondary structures of RNA3 and sgRNA3a. Here, the sgRNA3a would act as a “docking partner” that anneals to the newly synthesized (–) sense RNA3. Both, the BMV RdRp capability to participate in primer extension with sgRNA3a on (–) RNA3 templates as well as its potency to switch among RNA templates were demonstrated previously *in vitro* (Sztuba-Solińska et al., 2011a).

We focused our current study on analyzing the potential role of specific *cis*-acting RNA motifs in RNA3–sgRNA3a crossovers. Our recent data (Sztuba-Solińska et al., 2011a) suggested that the RNA3 position-dependent packaging element (PE) (Choi and Rao, 2003; Annamalai and Rao, 2006) focuses the RNA3–sgRNA3a crossovers. It was shown that removal of PE did not inhibit RNA3 accumulation in barley protoplasts (Choi and Rao, 2003). Here, we confirm that the deletion of a large portion of PE did not affect replication of RNA3 in protoplasts (Fig. 3) but it strongly debilitated recombination (transfection Δ PE-RNA3 × SG supported only 3% recombination frequency; Fig. 2A). Similarly, the Δ PE-RNA3 × Δ PE-SG transfection, in which both constructs were missing the PE motif, generated only three recombinants, all carrying the 5' *Bam*HI marker mutation. In contrast, when the same PE motif was deleted only in sgRNA3a (transfection Bbox-RNA3 × Δ PE-SG), this alteration was much less debilitating for recombination (reduction to 13%), likely as a combined effect with the mutated Bbox element (Fig. 2C) that was shown to increase recombination.

The observed effects could be due to disrupted interactions between the Δ PE-RNAs and the CP, suggesting a link between recombination and encapsidation (Annamalai and Rao, 2006; Annamalai et al., 2008). Previously, it was shown that partial PE deletion eliminated RNA3 packaging (Choi and Rao, 2003). Since PE is functional only in (+) strands we speculate that the lack of CP binding to this motif might disrupt the initial interaction between the (+) strands of RNA3 and sgRNA3a, which in normal conditions would be supported *via* CP–CP dimerization/oligomerization. BMV CP ability to bind small RNA motifs together with RdRp was previously proposed to regulate the timing of BMV RNA synthesis and viral encapsidation (Zhu et al., 2007). Additionally, BMV CP was shown to co-purify with BMV replicase (Bujarski et al., 1982), and both BMV CP and viral RNAs were found to co-localize at viral “replication factories” (Bamunusinghe et al., 2011; Schwartz et al., 2004; Diaz et al., 2012; Seo et al., 2012). The bound CP might then support RNA crossovers during replication inside the factories. In addition, the bound CP might create obstacles for the replicase complex and promote strand switching.

Opposite effects were observed after mutating another CP-binding element, the Bbox hairpin loop (Baumstrak and Ahlquist, 2001). This structured motif participates in the assembly of the BMV replicase complex (*via* interaction with protein 1a) as well as it binds CP molecules (Baumstrak and Ahlquist, 2001; Yi et al., 2009b). However, mutations within the CP-Bbox binding region did not repress BMV RNA accumulation *in vivo* (Yi et al., 2009a). Additionally, its proximity to the RNA3 polyA region, previously shown to concentrate the crossovers (Wierzchoslawski et al., 2004), is suggestive of its involvement in RNA3–sgRNA3a recombination. In our studies, the Bbox mutations debilitated recombination, but while occurring in sgRNA3a rather than in RNA3 (Fig. 2B). For the latter (Bbox-RNA3 × SG) the frequency maintained the wt level (42%) (Sztuba-Solińska et al., 2011a) with the majority of recombinants carrying all three marker mutations (32 out of 42 recombinants). This effect suggested the prevalence of sgRNA3a-directed primer extension (Fig. 6A).

Mechanistically, we speculate that the Bbox-bound CP can expose the 3' end in sgRNA3a, facilitating its annealing to another (–) sense RNA3 template (template switch) followed by the sgRNA3a-directed extension into the progeny (+) sense RNA3 (Fig. 6A). In addition, the sgRNA3a-bound CP might interact with the replicase complex that is already present at the subgenomic promoter, which would also facilitate primer extension. At the same time, CP binding at the internal RNA3 Bbox motif would create an obstacle for progressing RdRp supporting the inner strand switching process. In addition, the presence of the polyA tail in sgRNA3a primer might be essential. We have demonstrated that BMV RdRp can initiate at the polyA tail of sgRNA3a *in vitro* (Sztuba-Solińska et al., 2011a).

The results from reciprocal protoplast inoculations support these observations. The transfection with Δ PE-RNA3 × Bbox-SG practically eliminated recombination (Fig. 2C) which might be due to missing PE in RNA3. Along these lines, a reverse transfection with Bbox-RNA3 × Δ PE-SG generated recombinants that carried all three sgRNA3a markers; again reflecting the sgRNA3a-directed primer extension on (–) templates. Since the Bbox-RNA3 × Δ PE-SG experiment supported the crossovers near the 3' end of sgRNA3a we conclude that the unmodified sgRNA3a Bbox structure supported primer extension due to binding to both BMV CP and BMV replicase proteins. Additionally, the lack of CP binding to the modified Bbox in RNA3 likely removes the road block for BMV replicase, and thus prevents the RdRp from inner strand switching. The results from the Bbox-RNA3 × SG co-transfection experiment (76% recombinants with all three marker sites) agree with the lines of this hypothesis.

Previously, Yi et al. (2009a) reported that the Bbox motif in the 5' UTRs of BMV RNAs 1 and 2 mediates CP binding. Analogous motif was also reported at the 5' UTR of RNA3 (Pogue et al., 1992); however, its CP-binding activity was not reported. Here we show that mutations in the Bbox like element did not affect the level of RNA3 (+) strands in protoplasts (Fig. 3). Similar observations were reported by Pogue et al. (1992) after deleting the 5' Bbox like sequence from BMV RNA3. Apparently, this region does not participate in the initiation of RNA3 (+) strands. However, two co-transfections involving RNA3 and/or sgRNA3a 5'box-like mutants (5'box-RNA3 × 5'box-SG and 5'box-RNA3 × SG) dramatically debilitated recombination (none and one recombinant, respectively, per 100 clones; Fig. 2D). These results complement our previously published low recombination rates with the 3'-nested sgRNA3a derivatives that were lacking the 5' Bbox-like motif (Sztuba-Solińska et al., 2011a). The effect of the disruption of the 5' Bbox-like sequence on sgRNA3a–RNA3 recombination might be due to changes in the entire topology (structure and/or communication with other motifs) of the recombining RNAs, making them less

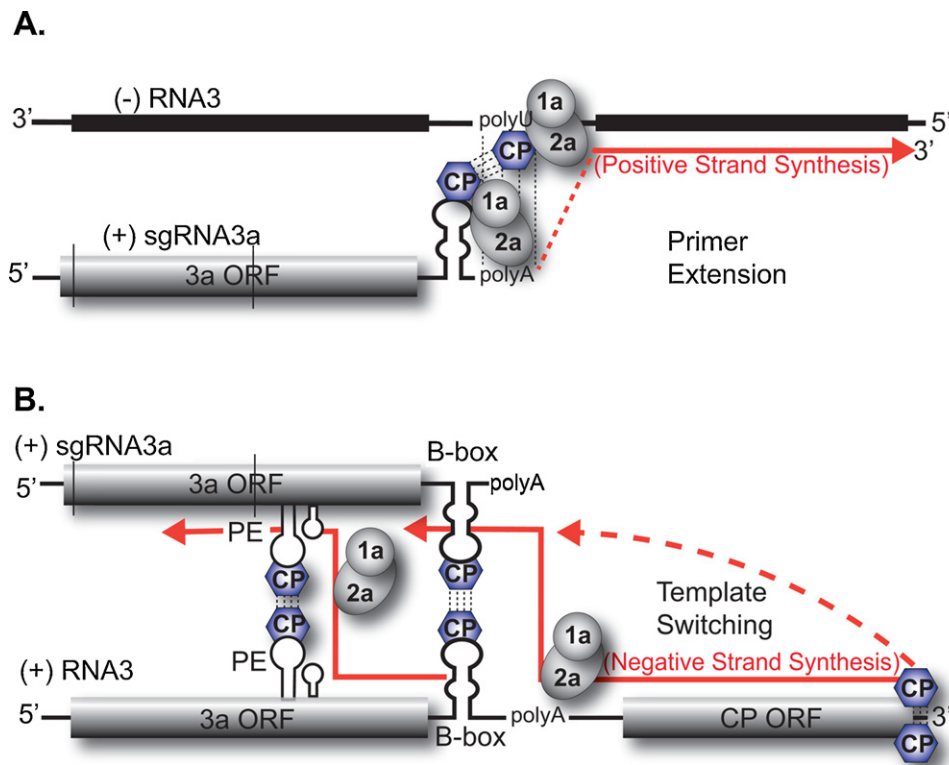


Fig. 6. Schematic models for proposed participation of CP molecules during recombination between BMV sgRNA3a and RNA3 during plus (model A) and minus (model B) strand syntheses. (A) Model of primer extension of sgRNA3a on (-) RNA3 templates. The BMV RdRp complex primes the hybridized sgRNA3a molecule and continues its translocation until completion on (-) RNA3 template. Both the Bbox element and the polyA tail facilitate the binding of 1a/2a proteins while the bound CP molecules (small blue hexagons) can bridge over with the RdRp complex bound to the subgenomic RNA promoter on (-) strand template. The CP binding might also loosen the original contact of the sgRNA3a/1a–2a complex. The 3' polyA tail and the corresponding internal polyU track are shown on the (+) and (-) strands, respectively. The 1a and 2a proteins of the RdRp complex are represented as shaded ovals. The polyA-polyU hybridization is represented as vertical dotted lines, whereas the red dotted line demonstrates the polymerase-priming events. (B) The strand-switching model during (-) strand synthesis. The binding of multimeric BMV CPs (represented by blue hexagons) to the PE sites (represented by two stem-loop structures) or to the intergenic Bbox motif sites (represented by single stem-loop structure) brings together both sgRNA3a and RNA3 (+) strand substrates via CP oligomerization. As yet another possibility, CP molecules bind to the stem loop C (SLC) at the 3' tRNA-like structure of the BMV RNA3 (+) strand and interact *in trans* with PE or Bbox sites in sgRNA3a, again bringing both molecules to a closer vicinity. The RdRp initiates the (-) strand synthesis at the 3' end of RNA3, and switches templates onto the sgRNA3a (+) strand at the CP-PE or CP-Bbox road-block bridges.

prone to crossovers. These possibilities will be a subject of further experimentation.

To substantiate our conjectures, an RNA3 mutant that cannot transcribe sgRNA4 and thus did not synthesize CP (CP0-RNA3) was tested. Here as well, the accumulation of BMV RNAs in protoplasts was not detectably affected. This agrees with earlier reports that blocking sgRNA synthesis had little effect on BMV RNA3 accumulation in barley protoplasts (Grzelishvili et al., 2005). The corresponding recombination frequency was at very low level (Fig. 2E). Thus, the lack of CP *per se* diminished recombination between RNA3 and sgRNA3a even if sequences of the *cis*-acting CP binding elements remained intact. Therefore, we conclude that CP plays an important role during homologous recombination between RNA3 and sgRNA3a.

To address further the role of RNA-CP interactions from the protein side, two CP domains mapped to bind RNA3 were altered by replacing codons of several amino acids with those for alanine, and then tested for recombination activity. One domain was the previously mapped Bbox binding region on CP (Yi et al., 2009a,b). Indeed, the amino acid substitutions diminished the interaction *in vitro* of the corresponding mutant CP preparation (CP-Bbox mutant) with the Bbox RNA probe (Fig. 5), and the recombination frequency in protoplasts was minimal (5%).

Yet another CP mutant (named CP-SLC) carried multiple amino acid replacements (again with the alanine residues) within a separate domain that was mapped to bind to the 3' SLC hairpin (Yi et al., 2009b), the RNA3 (-) strand replication signal (Chapman and Kao,

1999). Similar to CP-Bbox, the recombination frequency with CP-SLC was very low after co-transfecting with wt sgRNA3a (Fig. 2G). Collectively, these observations revealed that either the lack of CP or the disrupted binding of CP molecules to their cognate RNA binding signals debilitated significantly the recombination activity. One can speculate that the 3' SLC-bound CP increases the interaction between sgRNA3a and RNA3 molecules via long distance oligomerization (dashed arrow in Fig. 6B). Under this scenario, the strand switching during (-) strand synthesis could be facilitated. Alternatively, the 3' SLC-bound CP could boost the (-) strand synthesis (Chapman and Kao, 1999), which would increase the frequency of strand switching.

Filter binding assays revealed significant inhibition of CP-RNA binding for mutated sequences, as compared to the unchanged RNA or CP regions (Fig. 5). This was observed for point mutations within the Bbox element, for a large deletion within the PE region, as well as for CP amino acid substitutions within binding domains to Bbox and 3'-SLC elements. These observations confirm previous reports of Yi et al. (2009b) and Choi and Rao (2003). Most importantly, the strength of CP binding directly correlates with the recombination frequency, which further supports the predictions on the important contribution the CP plays during homologous recombination.

In conclusion, our data reveal important role of CP in homologous BMV RNA recombination and both mechanisms, the sgRNA3a-mediated primer extension and internal strand switching. As regarding the biological meaning of homologous crossovers with subgenomic components, these mechanisms can serve as

an efficient strategy that RNA viruses may use to diversify their RNA genomes and/or to guard the integrity of viral genome. It allows them to not only shuffle their genes so to adjust to ever-changing environment, but also to exploit subgenomic components as potential backup in case of extensive damage of their replication-competent genomic RNAs. The fact that BMV utilizes its multifunctional CP to orchestrate recombination proves once more the economical nature of virus life cycle under the limited resources. It is possible that CP-mediated recombination might be a common process among (+) stranded RNA viruses. The accumulating evidence demonstrates close proximity of viral RNA replication and CP translation inside the host cell (Annamalai et al., 2008; Seo et al., 2012). Thus, it is tempting to assume that RNA recombination processes are linked not only spatially but also they share protein factors. Yet, further studies are necessary to define more details of these mechanisms.

Acknowledgments

We would like to thank Stuart Hill for comments and discussions and Barbara Ball for assistance with figures. JJB was supported through a grant from the National Science Foundation (MCB-0920617) and through the Plant Molecular Biology Center at Northern Illinois University.

Appendix A. Supplementary data

Supplementary data associated with this article can be found, in the online version, at <http://dx.doi.org/10.1016/j.virusres.2012.10.001>.

References

- Annamalai, P., Rao, A.L.N., 2006. Packaging of Brome mosaic virus subgenomic RNA is functionally coupled to replication-dependent transcription and translation of coat protein. *Journal of Virology* 80, 10096–10108.
- Annamalai, P., Rofail, F., Demason, D.A., Rao, A.L., 2008. Replication-coupled packaging mechanism in positive-strand RNA viruses: synchronized coexpression of functional multigenome RNA components of an animal and a plant virus in *Nicotiana benthamiana* cells by agroinfiltration. *Journal of Virology* 82, 1484–1495.
- Bamunusinghe, D., Seo, J.-K., Rao, A.L.N., 2011. Subcellular localization and rearrangement of endoplasmic reticulum by Brome mosaic virus capsid protein. *Journal of Virology* 85, 2953–2963.
- Baumstrak, T., Ahlquist, P., 2001. The brome mosaic virus RNA3 intergenic replication enhancer folds to mimic a tRNA TCC-stem loop and is modified *in vivo*. *RNA* 7, 1652–1670.
- Bujarski, J.J., Dzanott, A.M., 1991. Generation and analysis of nonhomologous RNA–RNA recombinants in brome mosaic virus: sequence complementarities at crossover sites. *Journal of Virology* 65, 4153–4159.
- Bujarski, J.J., Hardy, S.F., Miller, W.A., Hall, T.C., 1982. Use of dodecyl-D-maltoside in the purification and stabilization of RNA polymerase from Brome mosaic virus-infected barley. *Virology* 119, 465–473.
- Chapman, M.R., Kao, C.C., 1999. A minimal RNA promoter for minus-strand RNA synthesis by the brome mosaic virus polymerase complex. *Journal of Molecular Biology* 286, 709–720.
- Choi, Y.G., Rao, A.L.N., 2003. Packaging of brome mosaic virus RNA3 is mediated through a bipartite signal. *Journal of Virology* 77, 9750–9757.
- Cocquet, J., Chong, A., Zhang, G., Veitia, R.A., 2006. Reverse transcriptase template switching and false alternative transcripts. *Genomics* 88, 127–131.
- Dedepsidis, E., Kyriakopoulou, Z., Pliaka, V., Markoulatos, P., 2010. Correlation between recombination junctions and RNA secondary structure elements in poliovirus Sabin strains. *Virus Genes* 41, 181–191.
- Diaz, A., Gallei, A., Ahlquist, P., 2012. Bromovirus RNA replication compartment formation requires concerted action of 1a's self-interacting RNA capping and helicase domain. *Journal of Virology* 86, 821–834.
- Draghici, H.-K., Varrelmann, M., 2010. Evidence for similarity-assisted recombination and predicted stem-loop structure determinant in potato virus X RNA recombination. *Journal of General Virology* 91, 552–562.
- Figlerowicz, M., 2000. Role of RNA structure in heteroduplex-mediated and site-specific nonhomologous recombination in brome mosaic virus. *Nucleic Acids Research* 28, 1714–1723.
- Figlerowicz, M., Nagy, P.D., Bujarski, J.J., 1997. A mutation in the putative RNA polymerase gene inhibits nonhomologous, but not homologous, genetic recombination in an RNA virus. *Proceedings of the National Academy of Sciences of the United States of America* 94, 2073–2078.
- Figlerowicz, M., Nagy, P.D., Tang, N., Kao, C.C., Bujarski, J.J., 1998. Mutations in the N terminus of the brome mosaic virus polymerase affect genetic RNA–RNA recombination. *Journal of Virology* 72, 9192–9200.
- Grdzlishvili VZ, Garcia-Ruiz, H., Watanabe, T., Ahlquist, P., 2005. Mutual interference between genomic RNA replication and subgenomic mRNA transcription in brome mosaic virus. *Journal of Virology* 79, 1438–1451.
- Hema, M., Kao, C.C., 2004. Template sequence near the initiation nucleotide can modulate Brome mosaic virus RNA accumulation in plant protoplasts. *Journal of Virology* 78, 1169–1180.
- Hu, W.S., Rhodes, T., Dang, Q., Pathak, V., 2003. Retroviral recombination: review of genetic analyses. *Frontiers in Bioscience* 8, D143–D155.
- Hurst, K.R., Ye, R., Goebel, S.J., Jayaraman, P., Masters, P.S., 2010. An interaction between the nucleocapsid protein and a component of the replicase–transcriptase complex is crucial for the infectivity of coronavirus genomic RNA. *Journal of Virology* 84, 10276–10288.
- Janda, M., French, R., Ahlquist, P., 1987. High efficiency T7 polymerase synthesis of infectious RNA from cloned Brome mosaic virus cDNA and effects of 5' extensions of transcript infectivity. *Virology* 158, 259–262.
- Kroner, P., Richards, D., Traynor, P., Ahlquist, P., 1989. Defined mutations in a small region of the Brome mosaic virus 2 gene cause diverse temperature-sensitive RNA replication phenotypes. *Journal of Virology* 63, 5302–5309.
- Nagy, P.D., Bujarski, J.J., 1993. Targeting the site of RNA–RNA recombination in Brome mosaic virus with antisense sequences. *Proceedings of the National Academy of Sciences of the United States of America* 90, 6390–6394.
- Nagy, P.D., Bujarski, J.J., 1994. Efficient system of homologous RNA recombination in Brome mosaic virus: sequence and structure requirements and accuracy of crossovers. *Journal of Virology* 69, 131–140.
- Nagy, P.D., Bujarski, J.J., 1996. Homologous RNA recombination in Brome mosaic virus: AU-rich sequences decrease the accuracy of crossovers. *Journal of Virology* 70, 217–225.
- Nagy, P.D., Bujarski, J.J., 1997. Engineering of homologous recombination hot-spots with AU-rich sequences in Brome mosaic virus. *Journal of Virology* 71, 3799–3810.
- Nagy, P.D., Bujarski, J.J., 1998. Silencing homologous RNA recombination hot spots with GC-rich sequences in Brome mosaic virus. *Journal of Virology* 72, 1122–1130.
- Negroni, M., Bus, H., 2000. Copy-choice recombination by reverse transcriptases: reshuffling of genetic markers mediated by RNA chaperones. *Proceedings of the National Academy of Sciences of the United States of America* 97, 6385–6390.
- Olsthoorn, R.C.L., Bruyère, A., Dzanott, A., Bujarski, J.J., 2002. RNA recombination in brome mosaic virus: effects of strand-specific stem-loop inserts. *Journal of Virology* 76, 12654–12662.
- Panaviene, Z., Nagy, P.D., 2003. Mutations in the RNA-binding domains of tombusvirus replicase proteins affect RNA recombination *in vivo*. *Virology* 317, 359–372.
- Pogue, G.P., Marsh, L.E., Connell, J.P., Hall, T.C., 1992. Requirements for ICR-like sequences in the replication of brome mosaic virus genomic RNA. *Virology* 188, 742–753.
- Ranjith-Kumar, C.T., Gutshall, L., Kim, M.J., Sarisky, R.T., Kao, C.C., 2002. Requirements for *de novo* initiation of RNA synthesis by recombinant flaviviral RNA-dependent RNA polymerases. *Journal of Virology* 76, 12526–12536.
- Rao, A.L.N., 2006. Genome packaging by spherical plant RNA viruses. *Annual Review of Phytopathology* 44, 61–87.
- Rao, A.L.N., 2007. Preparation and inoculation of mesophyll protoplasts from monocotyledonous and dicotyledonous hosts. *Current Protocols in Microbiology*, 16D.2.1–16D.2.8.
- Roda, R.H., Balakrishnan, M., Hanson, M.N., Wohrl, B.M., Le Grice, S.F., Roques, B.P., Gorelick, R.J., Bambara, R.A., 2003. Role of the reverse transcriptase, nucleocapsid protein, and template structure in the two-step transfer mechanism in retroviral recombination. *Journal of Biological Chemistry* 278, 31536–31546.
- Sambrook, J., Russell, D.W., 2001. *Molecular Cloning: A Laboratory Manual*. Cold Spring Harbor Laboratory Press, Cold Spring Harbor, NY.
- Seo, J.-K., Kwon, S.-J., Rao, A.L.N., 2012. A physical interaction between viral replicase and capsid protein is required for genome packaging specificity in an RNA virus. *Journal of Virology* 86, 6210–6221.
- Schwartz, M., Chen, J., Lee, W.M., Janda, M., Ahlquist, P., 2004. Alternate, virus-induced membrane rearrangements support positive-strand RNA virus genome replication. *Proceedings of the National Academy of Sciences of the United States of America* 101, 11263–11268.
- Shapka, N., Nagy, P., 2004. The AU-rich RNA recombination hot spot sequence of Brome mosaic virus is functional in tombusviruses: implications for the mechanism of RNA recombination. *Journal of Virology* 78, 2288–2300.
- Sivakumaran, K., Choi, S.-K., Hema, M., Kao, C.C., 2004. Requirements for Brome mosaic virus subgenomic RNA synthesis *in vivo* and replicase–core promoter interactions *in vitro*. *Journal of Virology* 78, 6091–6101.
- Suzuki, M., Hibi, T., Masuta, C., 2003. RNA recombination between cucumoviruses: possible role of predicted stem-loop structures and an internal subgenomic promoter-like motif. *Virology* 306, 77–86.
- Sztuba-Solińska, J., Dzanott, A., Bujarski, J.J., 2011a. Recombination of 5' subgenomic RNA3a with genomic RNA3 of Brome mosaic bromovirus *in vitro* and *in vivo*. *Virology* 410, 129–141.
- Sztuba-Solińska, J., Urbanowicz, A., Figlerowicz, M., Bujarski, J.J., 2011b. RNA–RNA recombination in plant virus replication and evolution. *Annual Review of Phytopathology* 49, 11.1–11.29.

- Wierchoslawski, R., Dziañott, A., Bujarski, J.J., 2004. Dissecting the requirement for subgenomic promoter sequences by RNA recombination of brome mosaic virus *in vivo*: evidence for functional separation of transcription and recombination. *Journal of Virology* 78, 8552–8564.
- Wierchoslawski, R., Urbanowicz, A., Dziañott, A., Figlerowicz, M., Bujarski, J.J., 2006. Characterization of a novel 5' subgenomic RNA3a derived from RNA3 of Brome mosaic bromovirus. *Journal of Virology* 80, 12357–12366.
- Yi, G., Letteney, E., Kim, Ch-H., Kao, C.C., 2009a. Brome mosaic virus capsid protein regulates accumulation of viral replication proteins by binding to the replicase assembly RNA element. *RNA* 15, 615–626.
- Yi, G., Vaughan, R.C., Yarbrough, I., Dharmiah, S., Kao, C.C., 2009b. RNA binding by the Brome mosaic virus capsid protein and the regulation of viral RNA accumulation. *Journal of Molecular Biology* 14, 314–326.
- Zhu, J., Gopinath, K., Murali, A., Yi, G., Hayward, S.D., Zhu, H., Kao, C.C., 2007. RNA-binding proteins that inhibit RNA virus infection. *Proceedings of the National Academy of Sciences of the United States of America* 104, 3129–3134.
- Zúñiga, S., Cruz, J.L., Sola, I., Mateos-Gómez, P.A., Palacio, L., Enjuanes, L., 2010. Coronavirus nucleocapsid protein facilitates template switching and is required for efficient transcription. *Journal of Virology* 84, 2169–2175.